

RESOLVING CARBON CONTRIBUTIONS IN A MANGROVE ESTUARY

A THESIS SUBMITTED TO
THE GLOBAL ENVIRONMENTAL SCIENCE
UNDERGRADUATE DIVISION IN PARTIAL FULFILLMENT
OF THE REQUIREMENTS FOR THE DEGREE OF

BACHELOR OF SCIENCE

IN

GLOBAL ENVIRONMENTAL SCIENCE

DECEMBER 2017

By
Elizabeth A. Dionne

Thesis Advisors

Henrietta Dulai
David Ho

We certify that we have read this thesis and that, in our opinion, it is satisfactory in scope and quality as a thesis for the degree of Bachelor of Science in Global Environmental Science.

THESIS ADVISORS

Associate Professor Henrietta Dulai
Department of Geology & Geophysics

Professor David Ho
Department of Oceanography

ACKNOWLEDGEMENTS

I would like to express my most sincere gratitude to my mentors, Dr. Henrietta Dulai and Dr. David Ho. Your wealth of knowledge, patience, and experience has been invaluable along my academic journey. It has been a pleasure to gain laboratory and field experience from such established experts.

This project was made possible by funding from the Undergraduate Research Opportunity Program and by the National Science Foundation through the Water Sustainability and Climate solicitation (EAR 1204572) and by the National Aeronautics and Space Administration (NNX14AJ92G) under the Carbon Cycle Science Program.

Additionally, I would like to thank Ben Hickman and my many formal and informal advisors who have guided my efforts throughout my time as an undergraduate. Finally, I would like to acknowledge the Oceanography office staff and my fellow Global Environmental Science students, who never hesitated to offer their assistance at every turn.

ABSTRACT

The global carbon cycle describes the flux of carbon between the atmosphere, terrestrial biosphere, and hydrosphere. Of this, the movement and storage of carbon dioxide is of great interest with the rapid changing of the climate. Mangrove forests act as a sink by removing CO₂ at a rate higher than other forests. Carbon becomes trapped in sediments, where it can be exported into aquatic estuarine environments. The aim of this study was to determine whether or not tidal pumping was a significant driver of carbon movement in an attempt to help a larger study quantify the flux of carbon flow along a mangrove lined estuary in Florida Everglades National Park. This site is located in the largest protected mangrove forest in the northern hemisphere. To accomplish this, we used the naturally occurring geochemical tracers radon and radium, and discrete measurements of dissolved inorganic carbon (DIC). Isotopic equilibrium values of Rn and Ra produced by the sediments were initially established to compare in situ measurements with. Multiple measurements of these isotopes in pore water were taken at four sites, varying in distance from tidal effects, in a mangrove lined estuary. This was done for both rising and falling tides, and during the dry and wet seasons. Our data suggest that water infiltrates and resides in sediments for about 1-4 tidal cycles. DIC was present in greater amounts during falling tides in the wet season but no well-defined link between the amounts of time water resides in pore spaces and DIC content could be established in both seasons. This could be because DIC enrichment of pore water due to in situ remineralization happens on time scales much shorter than what our method was able to capture.

TABLE OF CONTENTS

Dedication	ii
Acknowledgements	iii
Abstract	iv
List of Tables	v
List of Figures	vii
1.0 Introduction	1
1.1 Background	1
1.2 Tidal Pumping	4
2.0 Methods	6
2.1 Location & Site Descriptions	6
2.2 Application of Geochemical Tracers	8
2.3 Equations	10
2.4 Field Measurements	12
2.5 Analytical Measurements	13
3.0 Results	15
4.0 Discussion	25
4.1 Relation to Relevant Studies	25
4.2 Proof of Tidal Pumping	25
4.3 Groundwater DIC	26
4.4 Other Plausible Explanations of DIC Distribution	27
5.0 Conclusion	29
Appendix	30
Literature cited	32

LIST OF TABLES

Table 2.1. Site names, locations, average salinity.....	13
Table 3.1 Rn & Ra average equilibrium values determined from sediment.....	20
Table 3.2 Rn & Ra values with estimated water ages. Wet season.....	21
Table 3.3 Rn & Ra values with estimated water ages. Dry season	22
Table 3.4 Site carbon and alkalinity measurements. Wet season.	23
Table 3.5 Site carbon and alkalinity measurements. Dry season.	23

LIST OF FIGURES

Figure 1.1 Global Carbon Dioxide Budget	1
Figure 1.2 Mangrove production estimates	3
Figure 1.3 Mvmt of carbon btwn atmosphere, biosphere, and ocean	3
Figure 1.4 Diagram of tidal forcing	4
Figure 2.1 Map of Shark River tributary	7-8
Figure 2.2 Growth of Radon 222 from Radon 226	10
Figure 2.3 Uranium Decay Chain	10
Figure 2.4 Rad7 with attachment	12
Figure 2.7 Radium Delayed Coincidence Counter (RadDeCC)	14
Figure 3.1 Apparent age from ^{224}Ra plotted against grndwater sal. wet season.....	20
Figure 3.2 Apparent age from ^{224}Ra plotted against grndwater sal. dry season	20
Figure 3.3 Differences in seasonality in DIC at Cane Patch.....	21
Figure 3.4 Differences in seasonality in DIC at SRS 5	22
Figure 3.5 Differences in seasonality in DIC at SRS 6	22
Figure 3.6 Differences in seasonality in DIC at SR.....	23
Figure 3.7 Apparent age from ^{224}Ra (hrs) plotted against DIC content in wet season	24
Figure 3.8 Apparent age from ^{224}Ra (hrs) plotted against DIC content in dry season.....	24

CHAPTER 1. INTRODUCTION

1.1 Background

Every year carbon emitted from anthropogenic sources, totaling 41.9 GtCO₂ is added into the atmosphere (44%), land (30%), and oceans (26%) (Houghton et al. 2012). This circulation of carbon is well documented, however, it is not well quantified. For example, estimated flux between land and ocean stocks of carbon have uncertainties ranging upwards to 41% and 46% respectively (Li et al., 2016). In the case of mangrove forests, which are carbon sinks that assist in the global regulation of greenhouse gasses, more than half of the carbon fixed, 112-160 Tg C yr⁻¹, is unaccounted for (Maher, 2013; Boullion et al., 2008).

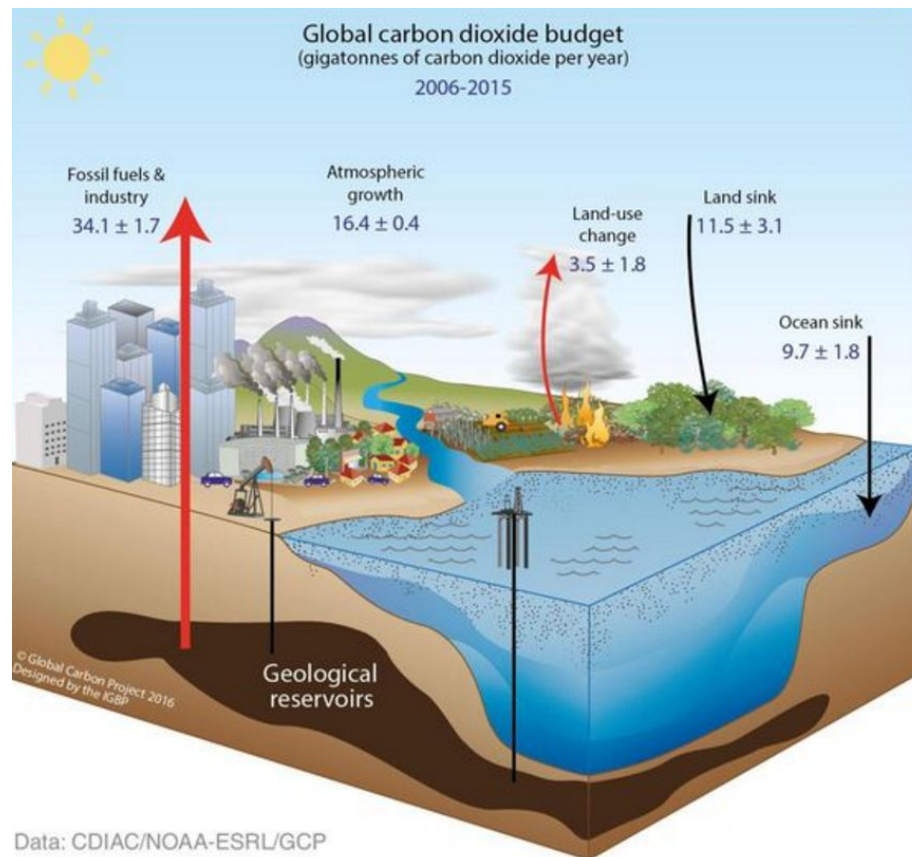


Figure 1.1 Global Carbon Dioxide Budget. (Carbon Dioxide Analysis Center, 2017).

Mangroves are a salt-tolerant species of shrub and tree that are located between tropical and subtropical latitudes 28°N and 28°S. Found at the interface of land and sea, these plants export a large amount of carbon from organic matter into coastal waters, and bury it into sediments. Litterfall adds $23 * 10^{12}$ g C per year to local sediments, and $46 * 10^{12}$ g C per year into coastal oceans (Jennerjahn & Ittekkot, 2004). Carbon is added to soil from root transport, or when leaves and stems fall from trees and are buried by soils (Fig 1.2). Mangroves in coastal wetlands are subject to tides, resulting in the soil being completely submerged for a portion of each day. The ensuing lack of oxygen slows decomposition of organic matter and prevents carbon from returning to the atmosphere. Current estimates show mangrove forests globally contributing 11% of the input of terrestrial carbon into the ocean, and 15% of total carbon exported into marine sediments (Jennerjahn, 2004; Bergamaschi, 2012).

The rapid accumulation and long-term burial of organic matter in sediments play an important part in the global carbon cycle. Carbon is buried in its organic form for an extended period, where it is subject to oxygen, nitrogen, and sulfate redox pathways (Howes, 1984). Via these remineralization processes, dissolved organic carbon (DOC) is transformed into dissolved inorganic carbon (DIC). The remaining carbon can be remineralized and mobilized by diffusion from sediments. Another way mobilization happens is by large burrowing organisms such as crabs. They assist in carbon mobilization by allowing oxygen-rich water to be pumped into sediments, and also flushing and irrigating burrows (Stieglitz et al. 2012). In addition, water fluxes through sediments driven by tides, called tidal pumping, may be an important yet an unexplored pathway of carbon transport too.

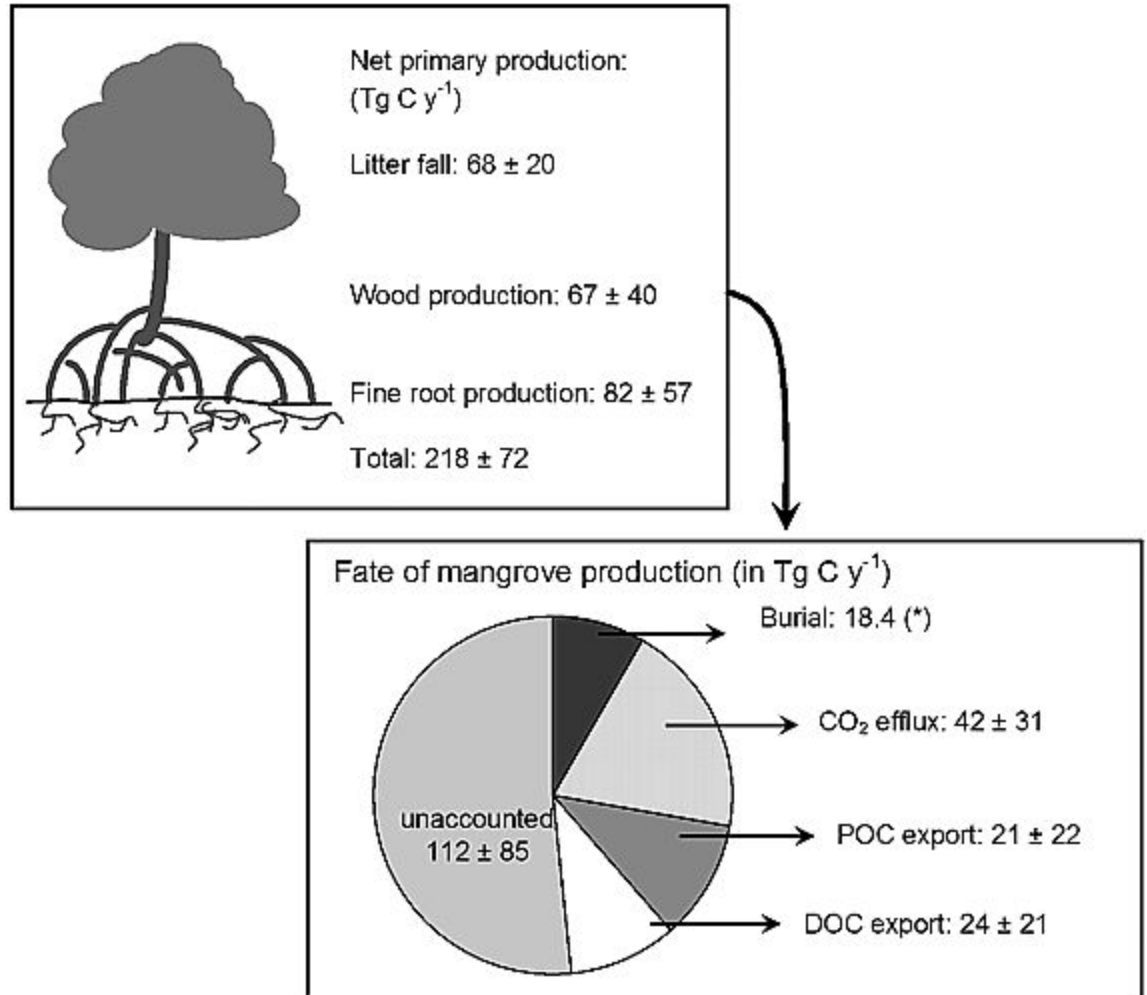


Figure 1.2 Mangrove production estimates (Boullion, 2008)

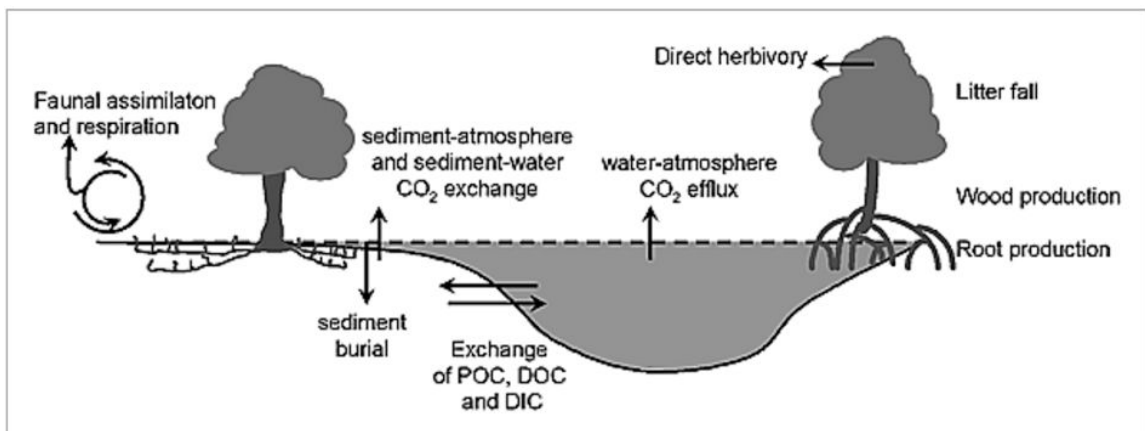


Figure 1.3 Movement of carbon between atmosphere, biosphere, and ocean. (Boullion, 2008)

1.2 Tidal Pumping

Tidal pumping is the mechanism by which seawater infiltrates the pore spaces of sediments during high tide, and then departs due to change in hydraulic gradient, drawing with it organic and inorganic matter into the marine environment during low tide (Nielson, 1990 & Robinson, 2007). This is one possible avenue of carbon export from buried organic matter. The alternating cycling of water brings new oxygen into a partially, or completely anaerobic environment. Tides have shown to have an impact on organic carbon mineralization in estuaries under aerobic conditions (Sasaki et al. 2009). This introduced oxygen, coupled with other electron acceptors, helps convert organic carbon into dissolved inorganic carbon (DIC); which becomes mobilized as the tide lowers and the water drains from the banks into open waters. As these tidal changes cover a large area, its probable large impact is a facet of our research.

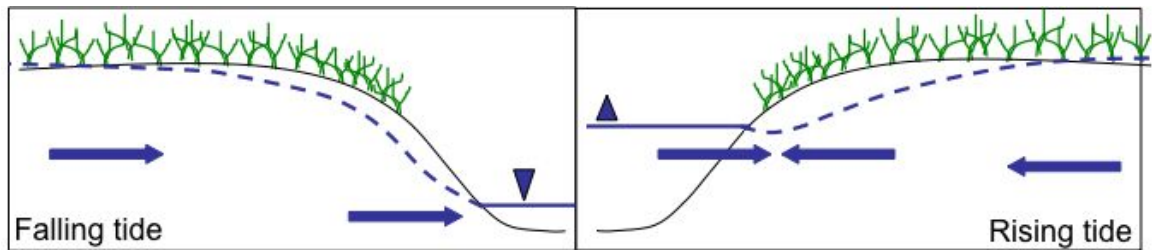


Figure 1.4. Diagram of tidal forcing.

The objectives of this study are to show that tidal pumping is one of the transport mechanisms of DIC, the time scale of water flow in the sediments, and to find evidence of carbon being transported from the sediments into open water. These objectives will be completed mainly by using geochemical tracers in a novel way to document the evidence of water infiltration and discharge across a spatially variable stretch of Shark River. With these measurements, the age of pore water can be determined and coupled with direct DIC and

nutrient measurements to model the flow of water through the river bank sediments over time.

CHAPTER 2. METHODS

2.1 Location & Site Descriptions

Everglades National Park is located on the southern end of Florida, encompassing 6,105 km², of which mangroves cover at an estimated 1700 to 2200 km². This is the largest protected mangrove forest in the northern hemisphere. Our sites are located along Shark River Slough, the largest drainage outlet in the Everglades. This estuary is lined by mangrove species (*Rhizophora mangle*), red mangrove, (*Avicennia germinans*), black mangrove, and (*Laguncularia racemosa*), white mangrove (Chen and Twilley, 1999). River flow through this wide, shallow basin is variable by season. During the dry season (November -May), there is a mean annual discharge of 0 m³s⁻¹. The wet season (June -October) has a mean annual discharge of 39 m³s⁻¹. (USGS Station 252230081021300). Shark River ranges in salinity from 0.3 to 35.8 (Pegram, 2013) with seasonal freshwater inputs. Under the vegetation is a layer of peat soils 1.5 to 5 m in depth, and below that a limestone platform (Wanlass et al., 1994).

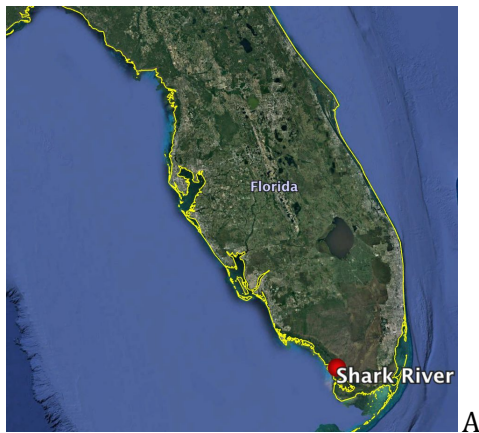
We studied four sites established by the Florida Coastal Everglades Long-Term Ecological Research Network (FCE-LTER). One site, 1.57 km inland from river mouth at the Gulf of Mexico, and another site 19.3 km inland from the river mouth. (Figure 3). Site names and their vegetation descriptions from furthest inland to the river mouth, as seen in figure 2.1.C and Table 1, are; Cane Patch, mainly populated by medium, dense spike rush vegetation. Shark River Slough 5 (SRS 5) is populated by red mangroves. Shark River Slough 6 (SRS 6), red mangrove, white mangrove, black mangroves. Shark River (SR) has almost exclusively red mangroves.

Tides at Shark River are semidiurnal with their amplitude dampening further inland. Tide fluctuations can reach as far as 30 km inland. At the study sites, tidal

fluctuations are as high as 1.0 m at SR, near the Gulf, and 0.3 m at Cane Patch, the site furthest inland (Figure 2.1).

Table 2.1 Site names, locations, average salinity.

Site name	Latitude	Longitude	Avg. Salinity
Cane Patch	25.42241	-80.94199	3.6
SRS 5	25.37702	-81.03235	17.34
SRS 6	25.36463	-81.07795	29
SR	25.35338	-81.10048	23.65



A



B



Figure 2.1. Map of Shark River tributary. A) Florida State. B) Everglades National Park. C) Map of study site. Google Earth & GIS.

2.2 Application of Geochemical Tracers

Determining the infiltration of surface water and its recirculation as pore water can be difficult, so the use of geochemical tracers was advantageous in our research. A geochemical, specifically, isotopic tracer, allows us to trace processes across various temporal and spatial scales. For this project, we utilized the naturally occurring isotopes of radon and radium. Both radon and radium are daughters of the uranium-thorium decay series (Fig 2.3). Both are conservative and diffuse continuously from sediments into

surrounding waters (Burnett et al. 2007), though radium is only released into brackish water due to its ion exchange reactions (Santons et al., 2010). Their short half-lives make them ideal for examining the short term movement of coastal waters (Dulaiova et al., 2005). Half-life ($t_{1/2}$) is 3.8 days for ^{222}Rn , and 11.3 and 3.7 days for ^{223}Ra and ^{224}Ra respectively.

Estimating the movement of water with radon can be done using discrete measurements or measurements done continuously at one location over time; however, the drawback of this method is that radon is a gas and its loss to the atmosphere will impact flux estimations (Burnett et al., 200). Water that has been recirculated in sediments will be more enriched in these isotopes than surface water that has been freshly introduced into the sediments. When that groundwater discharges from the sediments it takes radon and radium with it, therefore increased concentrations of radon and radium in the river suggests groundwater input either from the aquifer or tidal pumping.

Radon was employed to measure the residence times of surface water that infiltrated into the sediments within pore spaces. As the amount of time the water resides in a pore space increases, the amount of radon found in the water increases in a predictable manner (Fig 2.2). From the pore water radon distribution we can establish a temporal and spatial model to reconstruct the movement of water through the sediments. These measurements have been used to document the movement of DIC by advective tidal pumping rather than diffusive flux (Maher et al., 2013). Radium was used under the same principle. While radium has a much more complex chemistry because of its sorption to sediments in freshwater (Moore, 1996), our study sites were inundated with brackish and salty water so we could use radium the same way as radon, assuming that any produced radium would dissolve into pore water at a predictable rate.

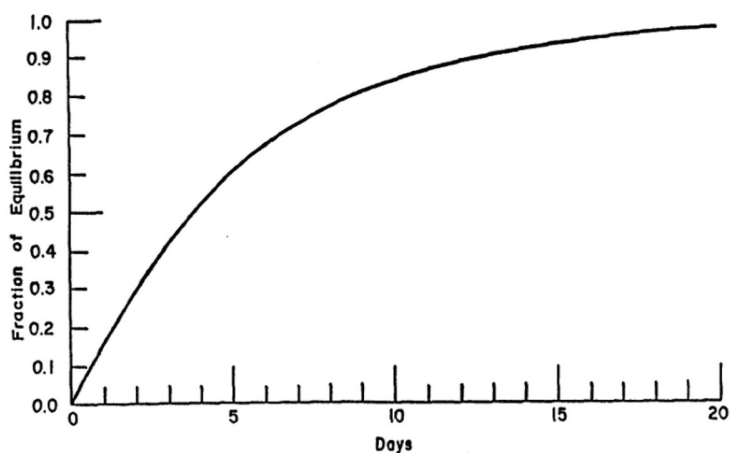


Figure 2.2. Growth of Radon 222 from Radon 226. Modified from USGS

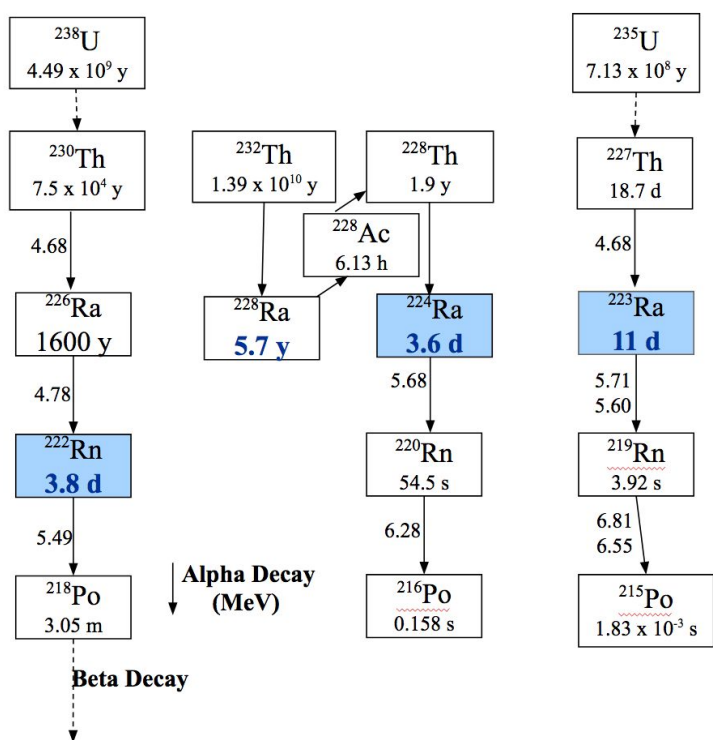


Figure 2.3. Uranium Decay Chain modified from USGS.

2.3 Equations

Apparent ages estimated from ^{222}Rn , ^{223}Ra , and ^{224}Ra were expressed based on the assumption that surface water with known isotope concentrations entered the sediment at

time (t_0) and at that moment started accumulating more of these isotopes and continued to do so until it reached equilibrium values or discharged back into the river. Rn and Ra activity at time (t) was measured in the field at various distances and depths from the banks to capture various groundwater flow paths. $t-t_0$ represents the apparent age.

$$\text{Apparent Age} = \ln\left(\frac{Rn_{eq} - (P * {}^{222}\text{Rn})}{Rn_{eq} - {}^{222}\text{Rn}}\right) * 3.66 \quad \text{Eq(1)}$$

Where $Rn_{(eq)}$ is the radon equilibrium value. P is the proportion of seawater. ${}^{222}\text{Rn}$ is measured radon (Bq/m).

$$Rn_{eq} = \frac{{}^{222}\text{Rn}_{\text{present}}}{1 - e^{-\frac{\ln(2)}{3.8} * t}} * t \quad \text{Eq(2)}$$

Rn_{eq} is the equilibrium value. ${}^{222}\text{Rn}_{\text{present}}$ is the amount of radon present, and t is time (days) sample was left to reach equilibrium.

$$Ra_{eq} = \frac{Ra_{pw}}{1 - e^{-\frac{\ln(2)}{I} * t}} * t \quad \text{Eq(3)}$$

Ra_{eq} is the equilibrium value of ${}^{223}\text{Ra} / {}^{224}\text{Ra}$. Ra_{pw} is the amount of ${}^{223}\text{Ra} / {}^{224}\text{Ra}$ present in pore water. I is the half life of ${}^{223}\text{Ra}$ (11.4) or ${}^{224}\text{Ra}$ (3.66).

$$\text{Apparent Age} = \ln\left(\frac{1 - Ra_{pw}}{Ra_{eq}}\right) / * \frac{-\ln(2)}{I} \quad 24 \quad \text{Eq(4)}$$

Ra_{pw} is the amount of ${}^{223}\text{Ra} / {}^{224}\text{Ra}$ present in pore water. Ra_{eq} is the equilibrium value. I is the half life of ${}^{223}\text{Ra}$ (11.4) or ${}^{224}\text{Ra}$ (3.66).

$$\text{Porosity} = 1 - \left(\frac{\text{Bulk Density}}{\text{Particle Density}}\right) * 100 \quad \text{Eq(5)}$$

Bulk density is the dry weight of sediments divided by volume, inclusive of pore spaces. Particle density is the weight per unit volume of the solid portion of soil.

$$C = C_0 * e^{-\lambda * t}, \quad \text{Eq(6)}$$

C is the measured concentration, C_0 is initial concentration (to be calculated) after the decay correction and t is the time elapsed since collection (in days), $\lambda = (0.693) / (t_{1/2}) = 0.181$, $t_{1/2} = 3.83$ days.

2.4 Field Measurements

Groundwater samples were taken at each site during low tide by using a push-point sampler and peristaltic pump. At increasing distances from the shore, the push-point sampler was inserted between 0.3 - 0.8 m into the ground. Withdrawn groundwater was first measured for temperature ($^{\circ}\text{C}$), conductivity (mS/cm), salinity, pH, and dissolved oxygen (% and mg/L) with a multiparameter sonde (YSI EXO). Then, water was pumped directly from the ground into 250 mL glass bottles, filling them completely and capped allowing for no air bubbles. At the end of each day, these samples were analyzed using the Rad7 H_2O system (Dulaiova, 2005) to measure radon activity.



Figure 2.4 Rad7 with attachments.

Variations of ^{222}Rn in surface water were also monitored at each site. Continuous measurements were taken from the riverbank at each mooring station using a RAD-Aqua (DurrIDGE Co., Inc.). These readings allow us to observe ^{222}Rn in the surface water column to know what infiltrates into the sediments.

While taking groundwater samples to measure radon, samples were also taken to measure dissolved organic carbon (DOC), DIC, and $\delta^{13}\text{C}$ of DIC content. Groundwater was collected into sample rinsed polypropylene syringes. Then filtered through a .45 micron

filter. A small amount of water was pushed through the filter initially to rinse it and the water was discarded. Samples were refrigerated and kept cool until processing. Dissolved inorganic carbon was analyzed at the Monterey Bay Aquarium Research Institute. Carbon isotopic composition of DIC was determined at the Rosenstiel School of Marine and Atmospheric Sciences

2.5 Analytical Measurements

Sediments found on the banks of Shark River are heterogeneous, so sediment was collected from each site in order to more accurately calculate radon and radium equilibrium concentrations, i.e., how much radon and radium does each different sediment composition produce if the water resides in it until radioactive ingrowth reaches equilibrium between the parent and daughter isotopes. After drying the sediment samples from each site in an oven, bulk density and particle density were measured to determine individual sediment porosity, equation (5). Then, the sediments were put into a 250 mL bottles to fill about $\frac{1}{4}$ of the bottle, the remainder was filled completely with radon and radium free water. Each sample was agitated twice a week for 21 days, at which point radon activity will have reached an equilibrium value (Cook et al. 2006). Radon measurements were then taken with the Rad7. This was repeated three to five times for each site sample. From these numbers radon equilibrium values were determined (Rn_{eq}) in Eq 2.

A RAD-7 with H₂O attachment, connected in a closed circuit was used to measure radon concentration in groundwater and in sediment filled bottles. The Wat-250 protocol was used for the 250 mL bottles. The protocol had one run made up of four recycles each lasting 15 minutes. During the protocol the sample is aerated and polonium activity is measured. The concentration of radon is determined based off the amount of polonium-218

activity, ^{218}Po ($t_{1/2}=3.05$ minutes). The field samples were then decay corrected to the time of sampling according to Eq 6.

Radium samples were collected from groundwater using a peristaltic pump for extraction. The water was collected into a container and passed through a column with pre-weighed manganese fiber at a rate less than 1 L min^{-1} (Moore & Reid, 1973). These fibers were rinsed with deionized water and were analyzed with a Radium Delayed Coincidence Counter (RaDeCC, Scientific Instruments; Moore & Arnold, 1996) (Fig 2.7). Manganese fibers were analyzed in the laboratory for ^{223}Ra and ^{224}Ra at four intervals. Initially the day we returned from the field, one week after collection, one month after collection, and lastly three months after collection. These counts were used to calculate excess radium activities as described by (Moore, 2008).



Figure 2.7. Radium Delayed Coincidence Counter (RaDeCC)

CHAPTER 3. RESULTS

Samples were taken from each site at different distances from the shore. Distances ranged from 0.5 m to 17 m as detailed in Table 3.2 Samples drawn during October, the wet season, were taken during the departing tide. Samples drawn during March, the dry season, were taken during the rising tide. River water and pore water salinity increased as we moved from the inland site, Cane Patch, to SR, the site 1.5 km from the Gulf of Mexico. Pore water salinities ranged from 0.3 to 29.5 in October 2016 and 1.4 to 34.5 in March 2017.

Table 3.1 Rn & Ra average equilibrium values determined from sediment.

Site	Rn (dpm/L)	Ra-223 (dpm/L)	Ra-224 (dpm/L)
Cane Patch	300	13653	47656
SRS 5	190	18009	83690
SRS 6	307	5254	16828
SR	107	11751	24171

Table 3.2. Site information for wet and dry season sampling. SP indicates pore water and R indicates river water samples.

October 2016					March 2017				
Site	ID	Distance Inland (m)	Time (UTC)	Salinity	Site	ID	Distance Inland (m)	Time (UTC)	Salinity
Cane Patch	SP 22	17	16:05	1.26	Cane Patch	SP 34	17	14:37	1.4
	SP 23	12	16:15	3.66		SP 35	12	15:15	2
	SP 24	7.6	18:15	5.43		SP 36	7.6	16:50	2.1
	SP 25	1.6	18:35	4.11		SP 37	1.6	15:50	1.94
	R3	0	19:30	0.27		SR 38	0	18:15	5.43
SRS 5	SP 26	1.3	13:00	17.99	SRS 5	SP 39	3	13:31	19.4
	SP 27	2.5	14:30	16.73		SP 40	3	14:15	17.25
	SP 28	4	16:05	17.3		SP 41	2	15:12	17.70
	R4	0	16:30	16.7		SP 42	1	16:00	18.81

SRS 6	SP 19	2	15:05	29.3	SRS 6	SP 43	0.25	14:20	29.52
	SP 20	2	15:30	29.49		SP 44	2	15:10	28.10
	SP 21	2	18:30	28.26		SP 45	2	16:37	29.77
	R1	0	13:00	23.7		SP 46	2	18:40	30.38
	R2	0	15:10	22.05					
SR	SP 29	0.5	18:45	28.65	SR	SP 48	0.5	13:35	34.46
	SP 30	0.5	14:15	29		SP 49	0.5	14:25	32.5
	SP 31	0.5	17:50	26.15		SP 50	0.5	16:05	32.8
	SP 32	0.5	14:30	28.38		SP 51	0.5	17:55	33.79
	SP 33	0.5	17:55	25.04					
	R5	0	14:10	25.5					

Tables 3.3 and 3.4 show the ^{222}Rn and $^{223,224}\text{Ra}$ values from in situ measurements. Pore water radon concentrations ranged from below detection levels to 31 dpm/L. Many porewater samples had less radon than the river water or even below detection limit and we suspected that some radon may have gotten lost by evasion from the sediments or during sample collection. Radium levels ranged from 50-98600 dpm/L for Ra-223 and 233-146250 dpm/L for Ra-224. Radon and radium equilibrium values are found in Table 3.1. From those values apparent ages were calculated using equation 1. There is a discrepancy between radon and radium ages, which we again, believe is because of radon loss by evasion. The difference is large in the October Cane Patch site (Table 3.3), and at every site during March (Table 3.4). Because of this, $^{223,224}\text{Ra}$ ages were used instead of ^{222}Rn . The apparent age calculations are not sensitive to <1 hour because such small changes in activity are hard to detect. On the upper end, the method is sensitive to ages up to about a few weeks, which represents 2-3 half-lives depending on the isotope used. In general, the radium ages showed the same pattern although the Ra-224 ages were consistently lower. Because of its shorter half-life, this isotope is more sensitive to the time scales of water circulation at the site.

Table 3.3 Rn & Ra values with estimated water ages. Wet season.

October 2016							
Site	ID	Rn-222 (dpm/L)	Ra-223 (dpm/L)	Ra-224 (dpm/L)	Rn Age (hrs)	Ra 223 Age (hrs)	Ra 224 Age (hrs)
Cane Patch	SP 22	31	5183	4017	15	118	14
	SP 23	4	83	233	2	2	1
	SP 24	7	50	500	4	1	2
	SP 25	9	167	533	4	3	2
	R3	-	167	533	-	3	2
SRS 5	SP 26	6	967	5867	12	20	16
	SP 27	1	10817	42217	2	307	232
	SP 28	0	13333	38950	0	434	188
	R4	-	2350	5550	-	49	15
SRS 6	SP 19	0.06	30367	68750	0	143	76
	SP 20	0.7	92933	146250	0	1045	460
	SP 21	0.1	46483	84133	0	247	103
	R1	-	150	6033	-	1	5
	R2	-	3050	5417	-	12	5
SR	SP 29	5	6617	16617	4	27	15
	SP 30	5	9117	31517	4	38	29
	SP 31	1	10917	21650	1	46	19
	SP 32	0	98600	137867	0	1687	313
	SP 33	7	71633	108550	6	497	160
	R5	-	2250	5817	-	9	5

Table 3.4 Rn & Ra values with estimated water ages. Dry season.

March 2017							
Site	Sample ID	Rn-222 (dpm/L)	Ra-223 (dpm/L)	Ra-224 (dpm/L)	Rn 222 Age (hrs)	Ra 223 Age (hrs)	Ra 224 Age (hrs)
Cane Patch	SP 34	84	10500	667	10	294	2
	SP 35	8	67	550	1	1	2
	SP 36	5	333	1017	1	7	4
	SP 37	4	2383	2417	1	50	8
	SR 38	-	3983	4017	-	16	3
SRS 5	SP 39	0	9383	23433	0	39	21
	SP 40	0	9500	34283	0	39	32

	SP 41	0	2583	3217	0	10	3
	SP 42	-	1950	2217	0	8	2
SRS 6	SP 43	1	4467	14550	0	100	43
	SP 44	0.6	3533	9467	0	77	26
	SP 45	0.4	-	-	0	-	-
	SP 46	0	-	-	0	-	-
SR	SP 48	4	11550	19983	1	4	3
	SP 49	1	50583	111950	0	48	64
	SP 50	0	-	-	0	278	-
	SP 51	0	-	-	0	-	-

On average, largest concentrations of DIC were found to be at SRS 6 (13884 $\mu\text{mol kg}^{-1}$) and SRS 5 (13378 $\mu\text{mol kg}^{-1}$) during October. Lowest concentrations were found at Cane Patch (7742 $\mu\text{mol kg}^{-1}$) and SR (6423 $\mu\text{mol kg}^{-1}$). There was approximately a 35% decrease in DIC at the Cane Patch and SR site between October and March. There was approximately a 23% decrease in DIC at SRS5 and SRS6 sites between October (Table 3.5) and March (Table 3.6).

Carbon stable isotope values were very consistent among sites and seasons ranging between 26-28 ‰. As such, carbon isotopes of DIC were not useful in identifying DIC derived from carbonate dissolution, and those that were produced by organic matter remineralization. The former would have a signature closer to 0 and the latter, based on $\delta^{13}\text{C}$ of mangrove litter of ~ 30 ‰ (Mahr et al., 2017).

Table 3.5 Site carbon and alkalinity measurements. Wet season.

October 2016					
Site	ID	DIC ($\mu\text{mol kg}^{-1}$)	Alkalinity ($\mu\text{mol kg}^{-1}$)	$\delta^{13}\text{C}$ of DOC	ODO%
Cane Patch	SP 22	7995	7032	-27	6.4
	SP 23	9447	6121	-28	3.7
	SP 24	16060	12128	-28	3.8

	SP 25	12901	9991	-28	3.2
	R3	-	-	-	43.4
SRS 5	SP 26	13353	9551	-28	5.2
	SP 27	13444	9910	-28	4.1
	SP 28	14854	10457	-28	5.3
	R4	-	-	-	58
SRS 6	SP 19	13332	10453	-28	4.7
	SP 20	14238	11662	-28	3.6
	SP 21	12566	9999	-	3.9
	R1	-	-	-	4.27
	R2	-	-	-	59.1
SR	SP 29	-	9711	-28	5.1
	SP 30	13836	9098	-27	4.2
	SP 31	6152	5200	-27	8.4
	SP 32	9827	7743		5
	SP 33	9315	6566	-27	7.4
	R5	-	-	-	66.4

Table 3.6 Site carbon and alkalinity measurements. Dry season.

March 2017					
Site	ID	DIC ($\mu\text{mol kg}^{-1}$)	Alkalinity ($\mu\text{mol kg}^{-1}$)	δ 13C DOC	ODO %
Cane Patch	SP 34	5081	4544	-26	1.4
	SP 35	6869	5837	-27	2
	SP 36	9109	7646	-27	1.9
	SP 37	9910	8300	-27	-
	SR 38	-	-	-	-
SRS 5	SP 39	12566	6647	-27	5.3
	SP 40	12335	9748	-27	5.9
	SP 41	12757	10214	-27	7.44
	SP 42	11331	8910	-27	-
SRS 6	SP 43	11471	9366	-27	5.5
	SP 44	13700	10817	-27	2.7
	SP 45	11037	9147		-
	SP 46	10385	8517	-27	-
SR	SP 48	4233	3998	-26	32.3
	SP 49	8285	7936	-27	-

	SP 50	7138	6879	-27	-
	SP 51	6035	5287	-27	-

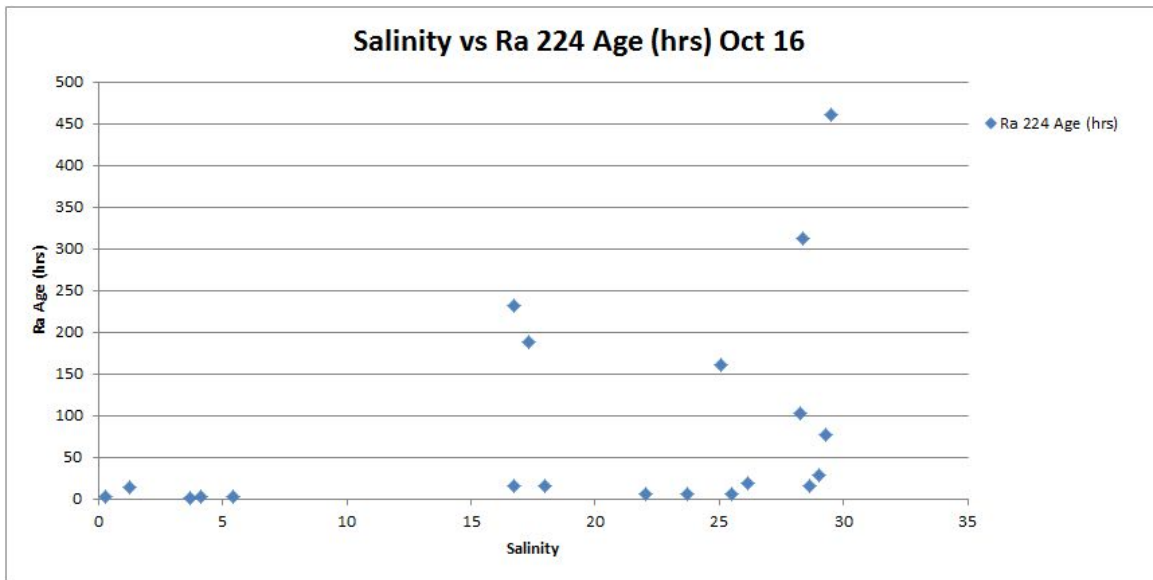


Figure 3.1 Apparent age from ^{224}Ra plotted against groundwater salinity in the wet season

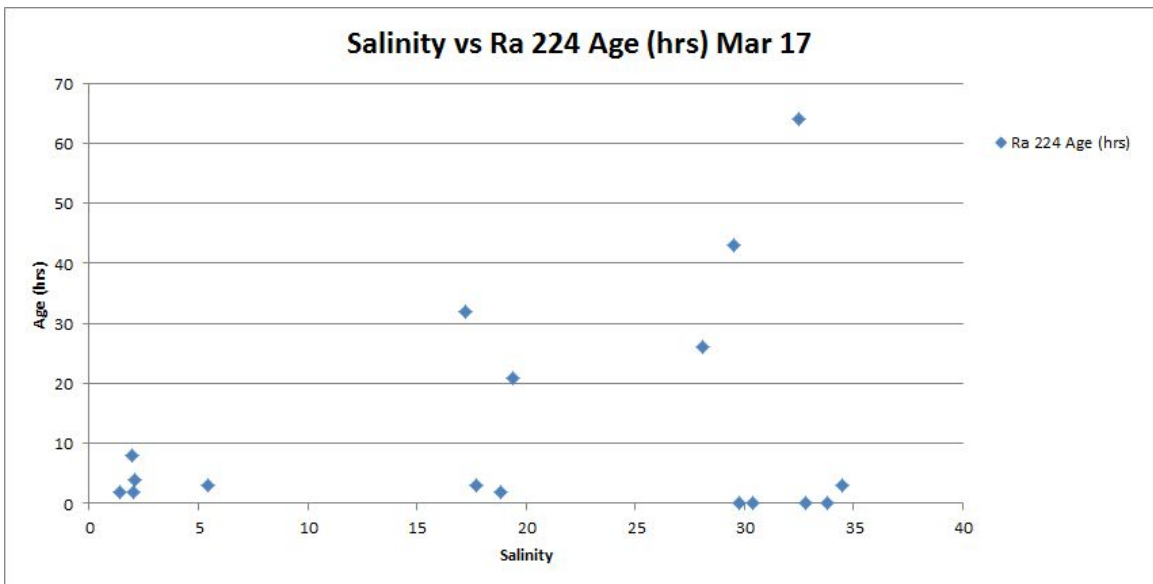


Figure 3.2 Apparent age from ^{224}Ra plotted against groundwater salinity in the dry season

Figures 3.1 and 3.2 reflect an increase in apparent ages in sites as salinity increases closer to the Gulf. While the tidal range is larger at sites closer to the Gulf, the sediments are inundated by saltier water which may desorb radium more effectively making sediment

seemingly older. We also noted in the field that sediments at Cane Patch released water much easier and therefore may be more permeable, hence experiencing more intense flushing, so younger pore water apparent ages. The water apparent ages range from 0 to few hundred hours in October and up to 64 hours in March. Considering that the tidal cycle produced high tide every 12.4 hours during our field excursions, it seems that water that infiltrates into the sediments resides there for at least 1-2 tidal cycles and does not drain immediately at the next low tide.

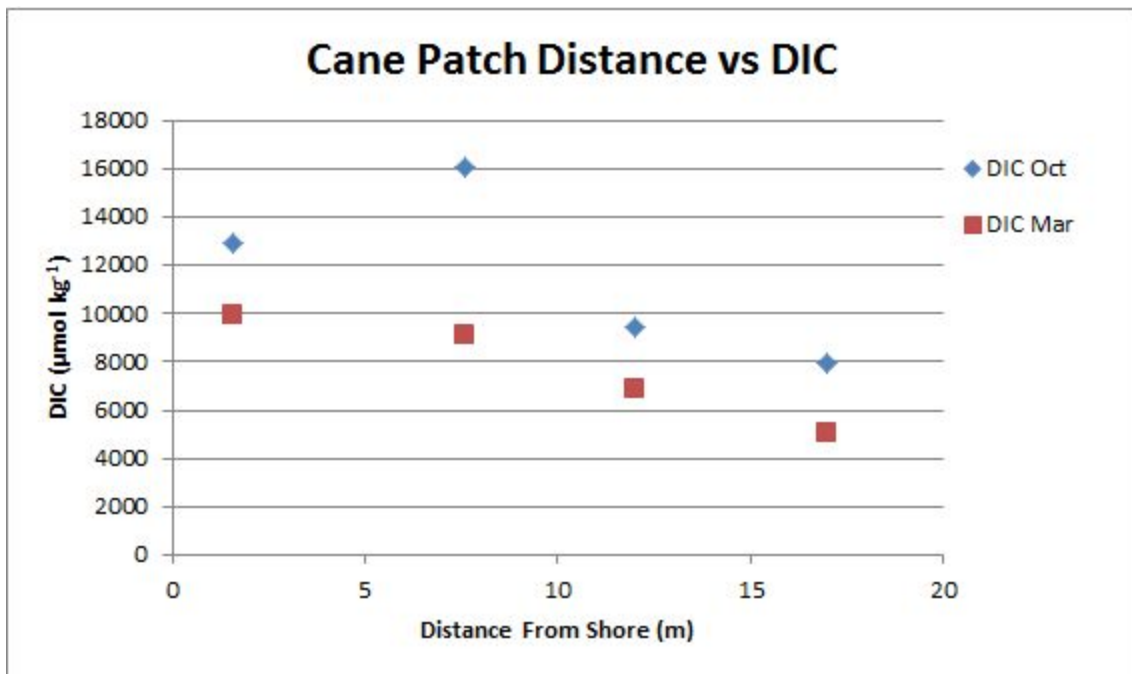


Figure 3.3 Differences in seasonality in DIC at Cane Patch.

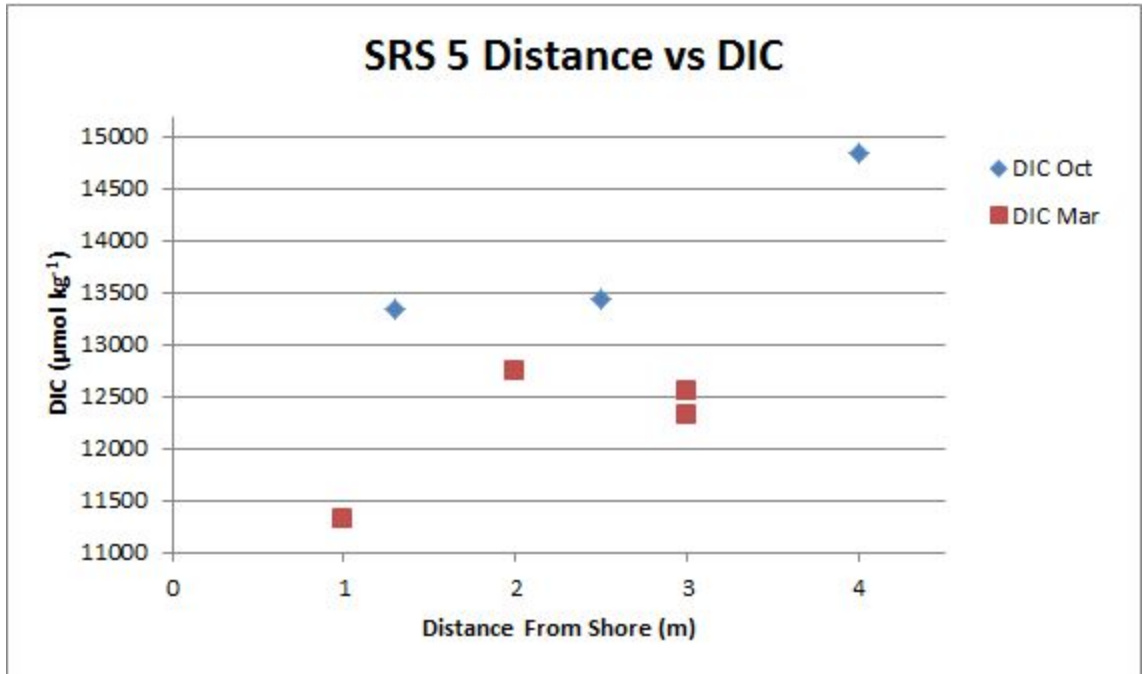


Figure 3.4 Differences in seasonality in DIC at SRS 5.

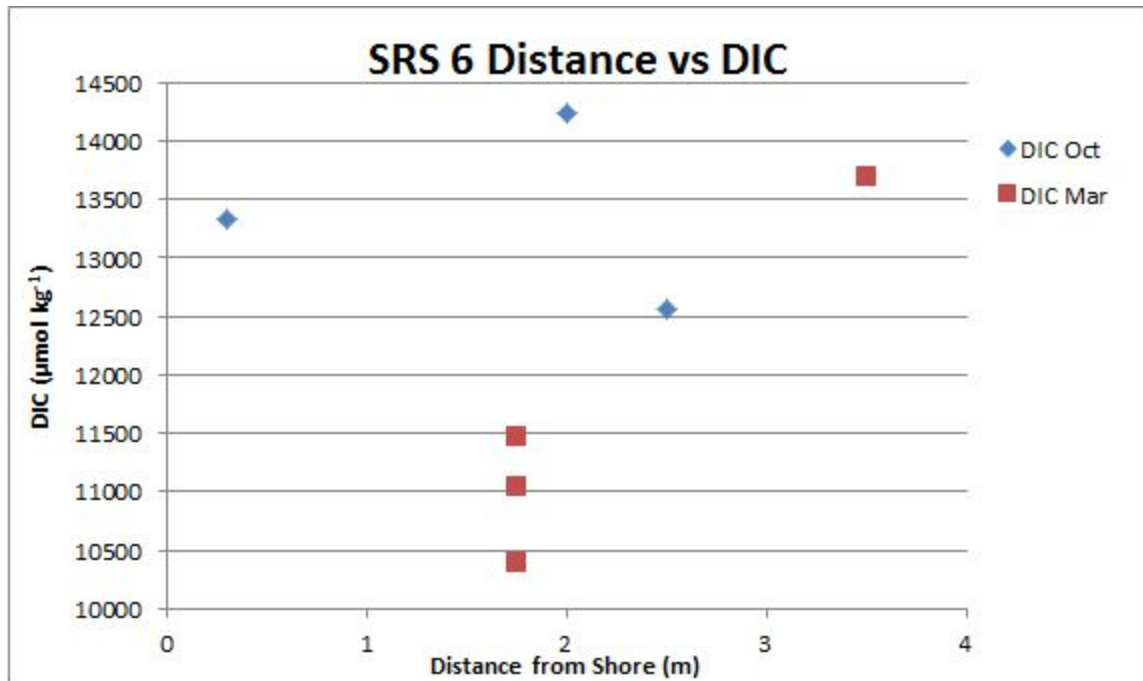


Figure 3.5 Differences in seasonality in DIC at SRS 6.

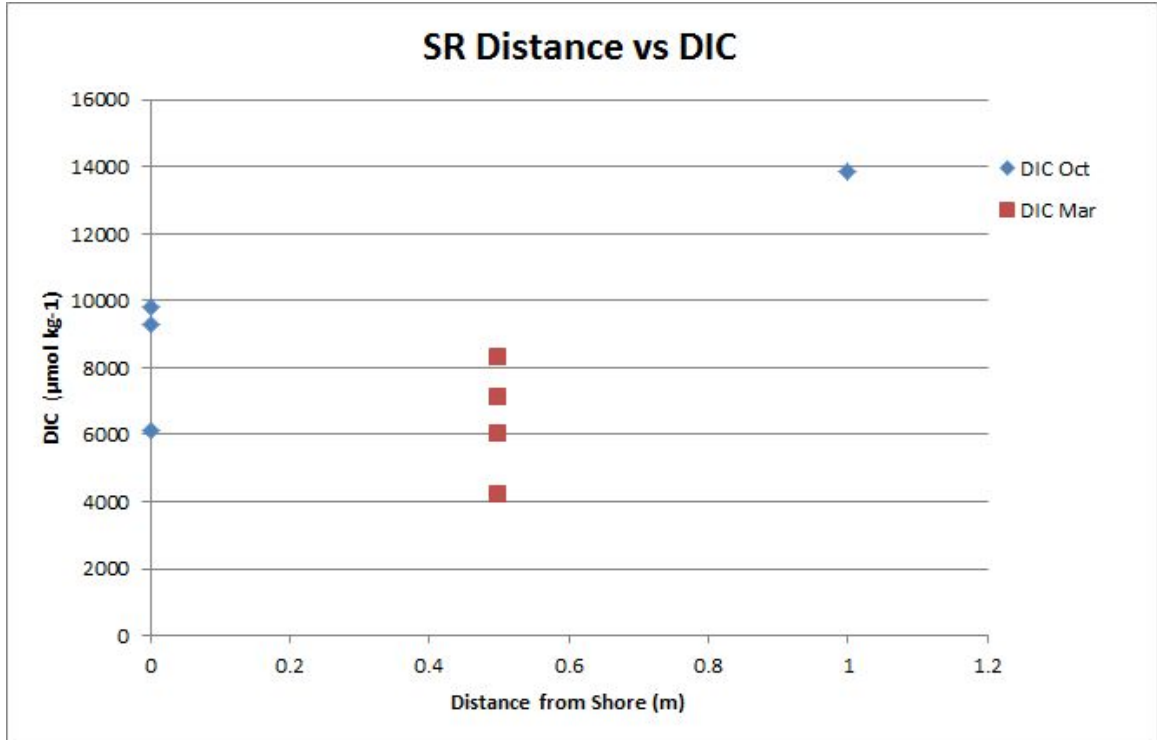


Figure 3.6 Differences in seasonality in DIC at SR.

Figures 3.3, 3.4, 3.5, and 3.6 show the differences in DIC content at SRS 5, SRS 6, and Cane Patch with distance from the river bank in the wet and dry seasons. Observed differences can be attributed to seasonal or tidal differences. Values in October are greater on average at all distances from the shore at every site. At Cane Patch DIC is higher near the mangrove dominated river bank but lower farther from the shore where small shrubs dominate the vegetation. At the other two sites, there is no clear trend of DIC with distance.

The apparent ages of water residing in pore spaces are shown in the below figure (Fig 3.7 & Fig 3.8). During the wet season, there is almost no correlation between the amount of time water spends in pore spaces and the amount of DIC it contains. The dry season does have a more pronounced correlation. Site SRS 6 however, does not show an increase in DIC as time increases during either season.

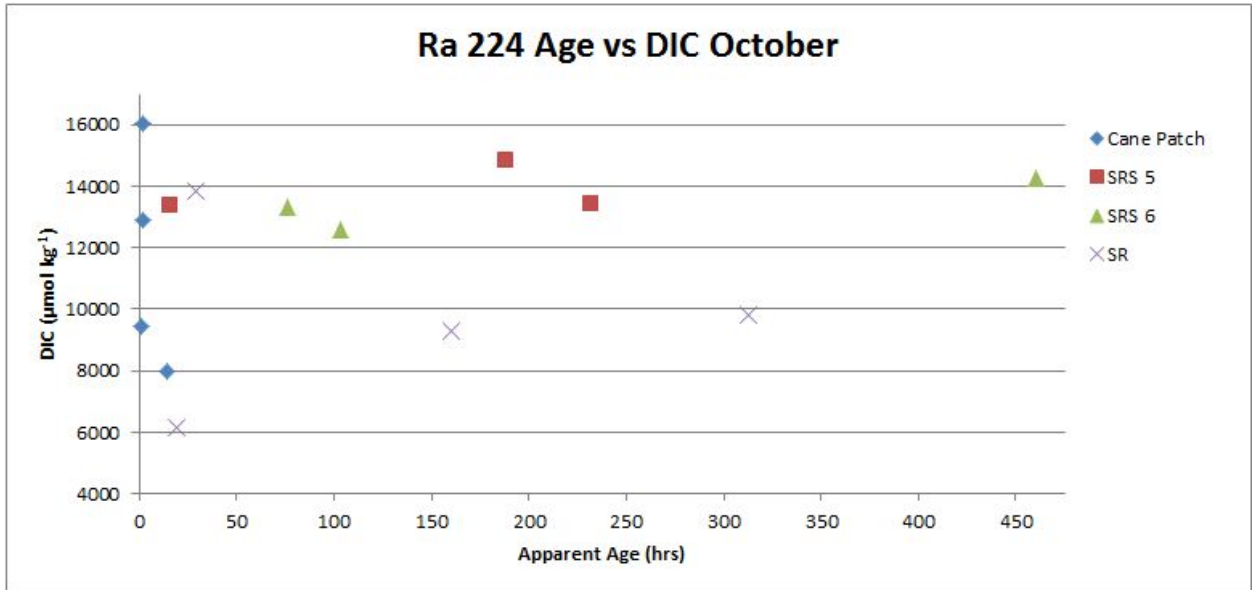


Figure 3.7 Apparent age from ^{224}Ra (hrs) plotted against DIC content in wet season.

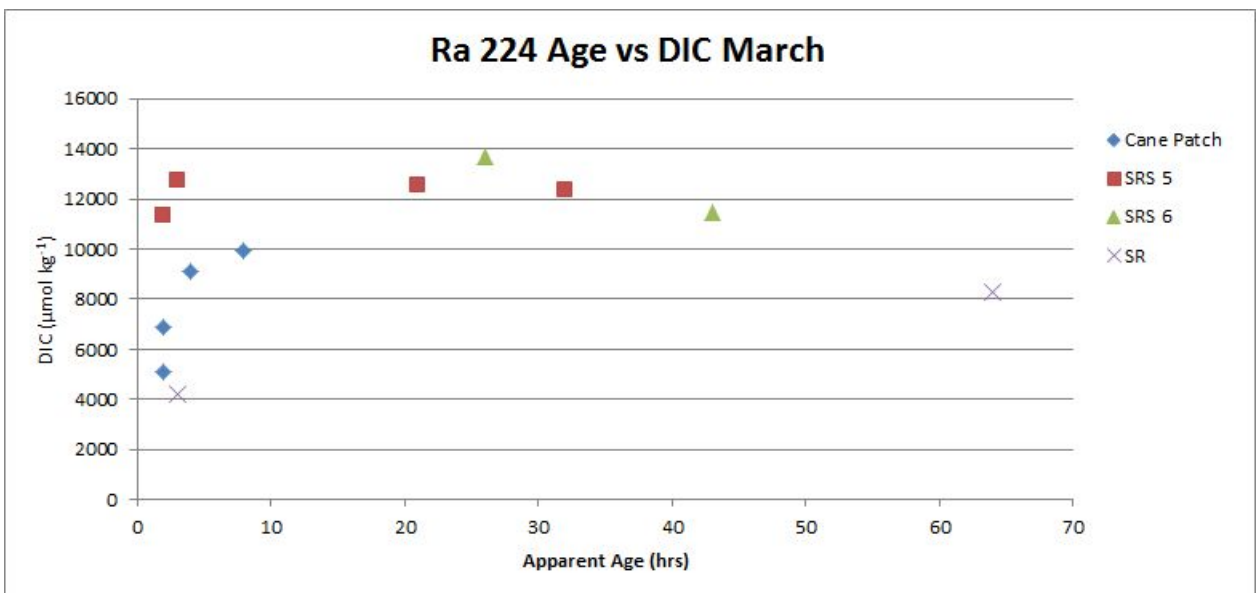


Figure 3.8 Apparent age from ^{224}Ra (hrs) plotted against DIC content in dry season.

CHAPTER 4. DISCUSSION

4.1 Relation to Relevant Studies

The concentrations of Ra found in pore water at our sites were comparable to concentrations found at Kangaroo Island, Australia (Gleeson, et al. 2013). Here it was found only 5 to 12% of incoming water infiltrated into the sediments during high tide and drained back at low tide. Additionally, crab burrowing was determined to increase hydraulic conductivity in otherwise impermeable sediment. The tunnel burrowing of crabs at Kangaroo Island mirrors the burrowing of crabs found in the Everglades area. They were observed at all of our sites, though no quantitative data was recorded in regards to their presence or actions they most likely influenced the amount of water infiltration at our study sites.

The DIC levels in our sites were approximately 5.2 times higher, and 7 times higher, than DIC found in the mangrove lined estuary in Ca Mau Province, Vietnam during the dry and wet seasons respectively (Kone & Borges, 2007). Our DIC measurements were however, comparable to the DIC content in pore water found during both wet and dry seasons in Timor Leste (Alongi et al., 2012). Additionally, our sites contained 3-7 times higher DIC amounts than six sites spanning the entire eastern coast of Australia (Sippo et al., 2016). The study performed in Timor was able to determine that DIC was moved through sediment by tides, by comparing DIC measurements of pore water with DIC measurements of draining water and finding them equivalent. In our study, the smell of sulfur was present when pumping groundwater samples, which indicates microbes utilizing third order redox pathways for respiration. Thus it could be concluded our sites are high in productivity. This indicates a limit to tidal exchange in deep sediment. If new tidally driven water were able to

reach all of our sampling sites, there would be no or little presence of sulfur due to the repetitive introduction of oxygen-rich water and the removal of oxygen-depleted water. However, it is still possible for water to cycle through the sediments and its oxygen to be depleted shortly after its introduction into the sediment.

4.2 Proof of Tidal Pumping

We observed radon in some, and radium enrichment over those observed in the river in all pore water samples. The radionuclide levels were, however, variable indicating a dynamic system. Especially important is the fact that Rn and Ra concentrations were lower than their equilibrium values. Assuming that the sediments are homogenous within each site producing isotopes at the same rate, we interpret the variable radionuclide levels by river water infiltration, i.e. river water with low activities of isotopes infiltrating into the sediments at high tide, then flowing within the sediments and collecting Rn and Ra, finally discharging at low tide. Indeed, some concentrations were as low as levels found in the river, and some were enriched several orders of magnitude. The radionuclide tracers, therefore, provide evidence that tidal pumping is moving water through the sediments.

During October the radium ages varied between 1 - 406 hours with an average of 83 hours. During March radium ages varied between 1 and 64 hours with an average of 16 hours. Shark River experiences a mixed semidiurnal tide, meaning 1 tidal period every 12.4 hours. From this we conclude that the layers of sediments we sampled are completely flushed on average every day in March over 1.5 tidal cycles, and on average every 3.5 days over seven tidal cycles in October. Figures 3.7, and 3.8 show almost no correlation between the apparent age of the water and its DIC content.

There was no clear pattern of apparent radium ages with distance from river bank, for example one could expect that shallower sediments or those closer to the river bank are flushed faster/more often due to tidal inundation and subsequent infiltration than the ones farther from the shore. There seemed to be a trend of ages getting younger with distance from the Gulf. This was assumed to be caused by the difference in permeability of the sediments as during sampling we noticed that pore water was hard to pump from the sediments at the sites closer to the Gulf but much easier at Cane Patch. This was not evaluated quantitatively and could be included in future research. To further support the interpretation of the water flow through sediments and discharging enriched in isotopes, Rn and Ra values in the river were elevated in comparison to expected ambient levels (data not shown).

4.3 Groundwater DIC

Figure 3.7 shows almost no correlation between the apparent age of the water and its DIC content. This is despite the fact the pore water DIC content is 2.5 times larger than river water, so pore water has to be enriched by DIC in the sediments. This discrepancy could be accounted for by very fast depletion of oxygen in the infiltrating water on a scale that was not captured by our sampling (mm to cm as opposed to 0.3-0.8 m). Dissolved oxygen content was below 10% in all pore water (Table 4 & 5) Most organic matter is probably remineralized using oxygen as an electron acceptor, and so pore water gets enriched in DIC very quickly. There are other possibilities for this discrepancy, but our sampling was not set up to address that.

4.4 Other Plausible Explanations of DIC Distribution

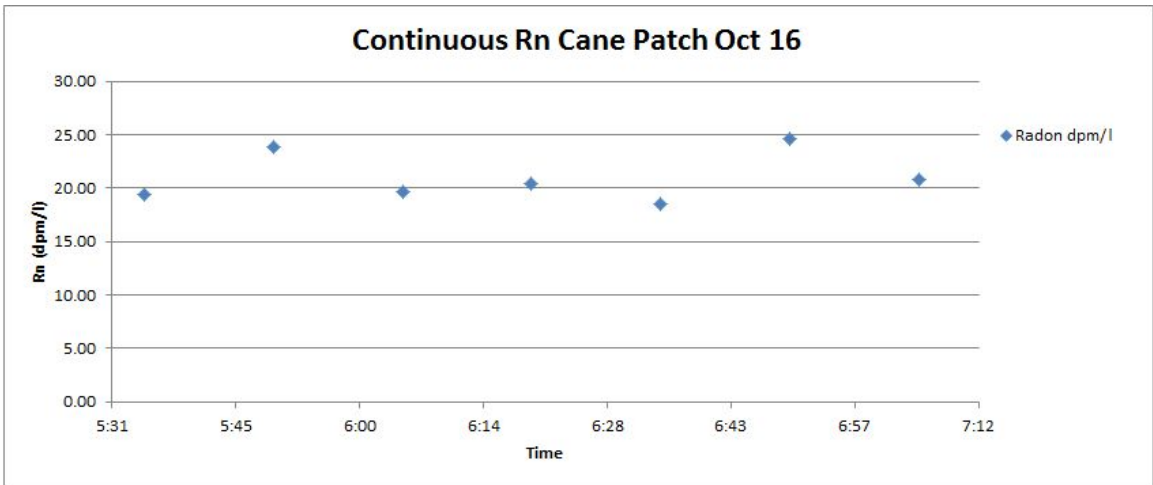
To more strongly support our claim of tides being one of the main drivers of DIC movement, we would have expected a positive correlation between apparent ages of water and DIC content in the October data set. From the data, it appears DIC content variance was more closely correlated with seasonal changes than with tidal fluctuations. Overall there was more dissolved inorganic carbon in the water during wet season than the dry one. This could be due to the introduction of fresh oxygen-rich water into the environment, allowing for more favorable microbial respiration reactions. Oxygen redox pathways allow for more dissolved inorganic carbon to be created.

In figures 3.3, 3.4, 3.5, and 3.6 the difference in DIC among sites could be explained by tidal forcing as well as seasonal variability. Samples taken in October were taken during the falling tide, and in March samples were taken during the rising tide. If tidal pumping is in fact an exporter of DIC into aquatic environments, then we would expect to see larger volumes in the falling tide. This is supported by data from each site though without data from the opposite tide during each season we cannot differentiate the culpability of tides compared with seasonal differences.

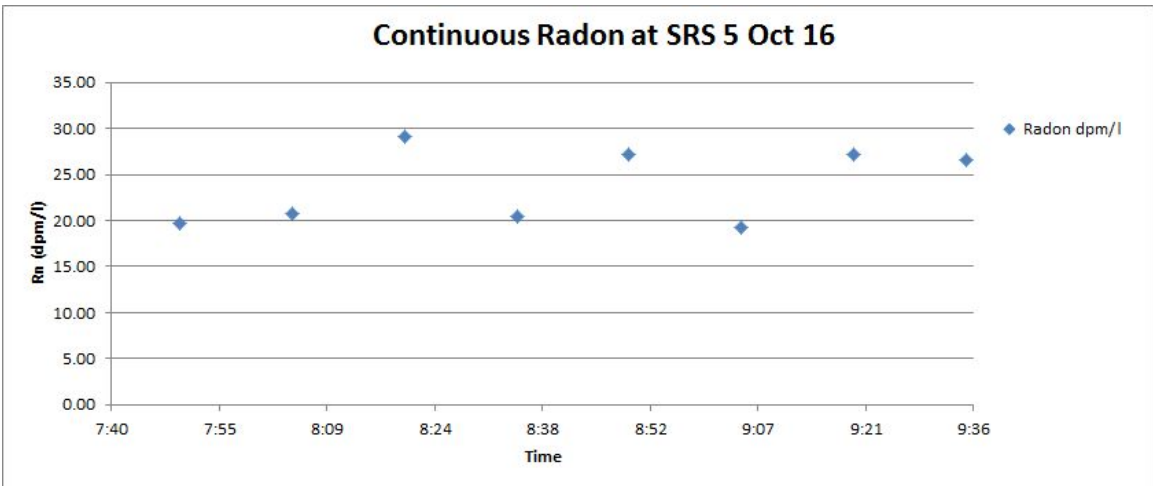
CHAPTER 5. CONCLUSION

Global budgets have shown that >50% of carbon fixed by mangroves is missing, and it has been suggested that DIC is exported from sediments into coastal waters due to the tides. In our research, we had expected that as DIC, Rn, and Ra depleted river water infiltrates the sediment at high tide, it flows through the layers of sediments, and over time it becomes enriched in DIC as well as Rn and Ra. Ideally, this would give us a positive correlation between DIC and apparent water ages. We were unable to show a strong positive correlation between the time water spends in pore spaces, and its DIC content in both March and October. At all sites there was a notable difference in DIC content between the seasons with the October, the rainy season, having more DIC. One reason a clear correlation between age of water and DIC is not seen in the wet season due to the increased amount of time to turnover pore space water. The rate of water exchange may be greater in March than in October. Radon was not a definitive tracers due to atmospheric evasion, but could be useful in future studies. This data is representative of a small portion of a larger study, so new information could change our outlook on the mechanics of tidal pumping the Shark River estuary.

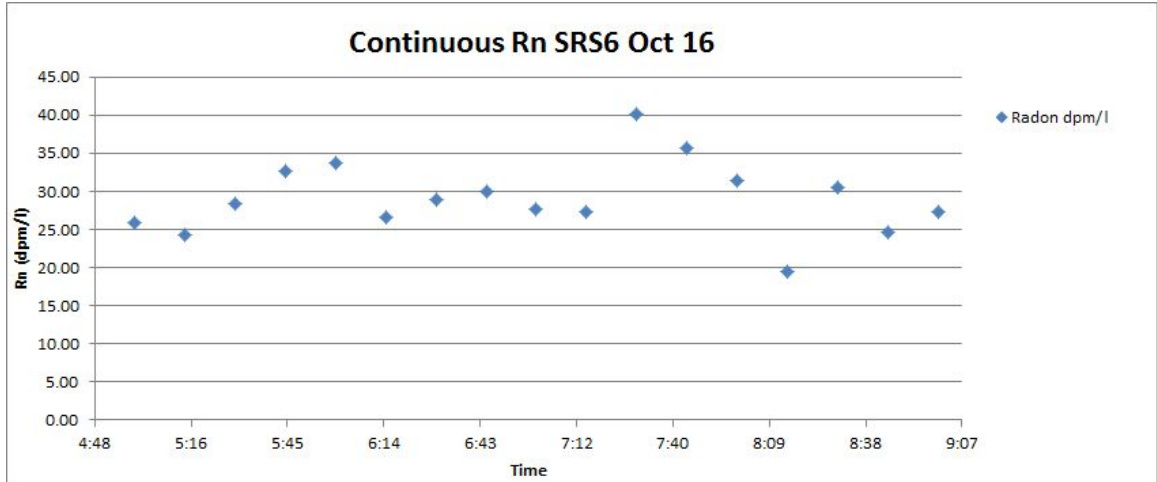
APPENDIX I



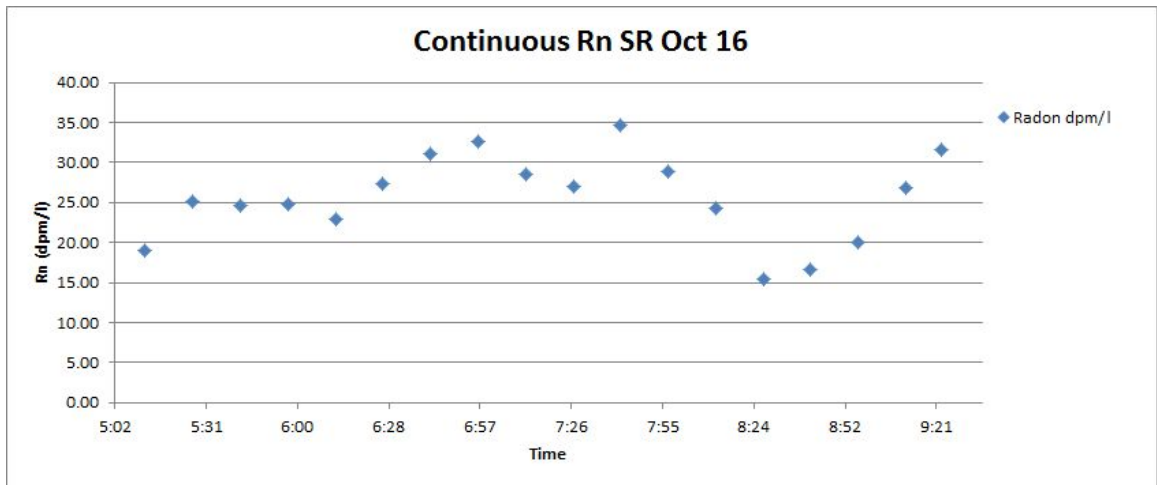
Continuous ^{222}Rn measurements taken of surface waters at Cane Patch.



Continuous ^{222}Rn measurements taken of surface waters at SRS 5



Continuous ^{222}Rn measurements taken of surface waters at SRS 6



Continuous ^{222}Rn measurements taken of surface waters at SR

REFERENCES

Literature Cited

Alongi, D.M., de Carvalho, N.A., Amaral, A.L. et al. *Biogeochemistry* (2012) 109: 151.
<https://doi-org.eres.library.manoa.hawaii.edu/10.1007/s10533-011-9616-9>

Armstrong, F., Steams, C., Strickland, J., (1967) The measurement of upwelling and subsequent biological process by means of the technicon autoanalyzer® and associated equipment. *Deep Sea Research and Oceanographic Abstract*, Elsevier (1967), pp. 381-389

Bergamaschi, B., Krabbenhoft, D., Aiken, G., Patino, E., Rumbold, D., and Orem, W.; (2012). Tidally Driven Export of Dissolved Organic Carbon, Total Mercury, and Methylmercury from a Mangrove-Dominated Estuary. *Environmental Science and Technology* 2012.

Bouillon, S., Borges, A. V., Castañeda-Moya, E., Diele, K., Dittmar, T., Duke, N. C., Kristensen, E., Lee, S. Y., Marchand, C., Middelburg, J. J., Rivera-Monroy, V. H., Smith, T. J., and Twilley, R. R.: Mangrove production and carbon sinks: A revision of global budget estimates, *Global Biogeochem. Cy.*, 22, GB2013, 10.1029/2007GB003052, 2008a.

Burnett, & Dulaiova. (2003). Estimating the dynamics of groundwater input into the coastal zone via continuous radon-222 measurements. *Journal of Environmental Radioactivity*, 69(1), 21-35.

Chen, R., Twilley, R.R., (1999). Patterns of mangrove forest structure and soil nutrient dynamics along the Shark River Estuary, Florida. *Estuaries*, 22 (1999), pp. 955-970

Gleeson, J., Santos, I., Maher, D., Golsby-Smith, L., (2013). Groundwater–surface water exchange in a mangrove tidal creek: Evidence from natural geochemical tracers and implications for nutrient budgets,. *Marine Chemistry*. 156. .
10.1016/j.marchem.2013.02.001,.

Howes Brian L. , Dacey John W. H. , King Gary M. , (1984), Carbon flow through oxygen and sulfate reduction pathways in salt marsh sediments, *Limnology and Oceanography*, 5, doi: 10.4319/lo.1984.29.5.1037.

Jennerjahn, T.C. & Ittekkot, V. *Naturwissenschaften* (2002) 89: 23.
<https://doi-org.eres.library.manoa.hawaii.edu/10.1007/s00114-001-0283-xg>

Koné, Y.J., Borges, A.V., (2007). Dissolved inorganic carbon dynamics in the waters surrounding forested mangroves of the Ca Mau Province (Vietnam), In *Estuarine, Coastal and Shelf Science*, Volume 77, Issue 3, 2008, Pages 409-421, ISSN 0272-7714,
<https://doi.org/10.1016/j.ecss.2007.10.001>.

Nielson, P.; (1990). Tidal dynamics in the water table in a beach. *Water Resources Research*, 26 (1990), pp. 2127-2134

Maher, D. T., Santos, I. R., Golsby-Smith, L., Gleeson, J., and Eyre, B. D.: Groundwater-derived dissolved inorganic and organic carbon exports from a mangrove tidal creek: The missing mangrove carbon sink?, *Limnol. Oceanogr.*, 58, 475–488, doi:10.4319/lo.2013.58.2.0475, 2013.

Maher, D. T., I. R. Santos, K. G. Schulz, M. Call, G. E. Jacobsen, and C. J. Sanders (2017), Blue carbon oxidation revealed by radiogenic and stable isotopes in a mangrove system, *Geophys. Res. Lett.*, 44, 4889–4896, doi:10.1002/2017GL073753.

Moore, W. S., and R. Arnold (1996), Measurement of ²²³Ra and ²²⁴Ra in coastal waters using a delayed coincidence counter, *J. Geophys. Res.*, 101(C1), pp. 1321–1329, doi:10.1029/95JC03139.

Pergram, Kathy. SOFIA - Surface Water Discharge and Salinity Monitoring of Coastal Estuaries in Everglades National Park - Discharge and Salinity, 2013.
https://sofia.usgs.gov/publications/papers/swdis_salmon/discharge_salinity.html

Robinson, L; Barry, D.A; (2007). Effect of tidal forcing on a subterranean estuary. *Advances in Water Resources* Vol 20, Issue 4, April 2007, pages 851-865.

Sasaki, A., Hagimori, Y., Nakatsubo, T. et al. *Ecol Res* (2009) 24: 723.
<https://doi-org.eres.library.manoa.hawaii.edu/10.1007/s11284-008-0545-6>

Sippo, J. Z., D. T. Maher, D. R. Tait, C. Holloway, and I. R. Santos (2016), Are mangroves drivers or buffers of coastal acidification? Insights from alkalinity and dissolved inorganic carbon export estimates across a latitudinal transect, *Global Biogeochem. Cycles*, 30, 753–766, doi:10.1002/2015GB005324.

Stieglitz, T., Clarck, J., Hancock, G., (2012). The mangrove pump: the tidal flush of animal burrows in a tropical mangrove forest determined from radionuclide budgets. *Goechim. Cosmochim. Acta*, 102 (2013), pp. 12-22